Research Square

Preprints are preliminary reports that have not undergone peer review.
They should not be considered conclusive, used to inform clinical practice,
or referenced by the media as validated information.

Femoral medullary composition in advanced post mortem decomposition: agreement of attenuation-based volumetric fractions across two PMCT reconstruction protocols

Pierrick Nègre[2]

pierrick.negre@chu-martinique.fr

Centre Hospitalier Universitaire de Martinique

Sarah Chaigneau[1]

Centre Hospitalier Universitaire de Toulouse

Fabrice Dédouit[1]

Centre Hospitalier Universitaire de Toulouse

Norbert Telmon[1]

Centre Hospitalier Universitaire de Toulouse

Frédéric Savall[1]

Centre Hospitalier Universitaire de Toulouse

Research Article

Keywords: post mortem computed tomography, bone marrow, image segmentation, decomposition, Radiological Alteration Index, forensic anthropology

Posted Date: November 4th, 2026

DOI: https://doi.org/10.21203/rs.3.rs-11309742/v1

License: This work is licensed under a Creative Commons Attribution 4.0 International License.
Read Full License

Additional Declarations: No competing interests reported.

Abstract

In advanced decomposition, conventional *post mortem* markers become progressively less informative, whereas bone and medullary content remain comparatively preserved. This retrospective study assessed whether femoral medullary composition can be quantified consistently on *post mortem* computed tomography (PMCT) using a semi-automated segmentation approach and whether attenuation-based volumetric fractions are associated with cadaveric alteration. PMCT examinations from 100 decomposed forensic cases (199 femora) were analysed with the SegMed module in 3D Slicer. Eight medullary fractions were quantified using soft-tissue (ST) and bone (BN) reconstruction protocols. Agreement was evaluated using intraclass correlation coefficients (ICCs), paired Wilcoxon tests and Bland–Altman analysis; associations with the Radiological Alteration Index (RAI) and estimated *post mortem* interval (PMI) were assessed using Spearman correlations with Benjamini–Hochberg correction. Agreement between ST and BN reconstructions was excellent for gas, fat-like marrow, fluid and intermediate-density fractions (ICCs > 0.94), despite small systematic offsets, whereas agreement was lower for residual medullary content on the right (ICC = 0.52) and unstable for debris. Gas fractions were positively associated with RAI, whereas fluid and intermediate-density fractions were negatively associated ($|\rho|$ approximately 0.25–0.37). No volumetric fraction was significantly associated with estimated PMI after correction. Semi-automated PMCT segmentation therefore yielded consistent measurements of the principal femoral medullary fractions across the two reconstruction protocols evaluated. These fractions are candidate quantitative markers of radiological cadaveric alteration, but their value for elapsed-time estimation requires validation in cohorts with more accurately known PMIs.

Introduction

Estimating *post mortem* changes becomes increasingly difficult as decomposition advances because early cadaveric signs disappear and late changes are strongly influenced by environmental and individual factors [1–4]. In advanced decomposition and partial skeletonisation, bone may remain one of the most durable substrates available for forensic examination, although it also undergoes progressive physicochemical modification [5, 6]. The medullary cavity of long bones is of particular interest because it is physically protected by the cortex and because bone marrow may persist after substantial soft-tissue degradation [7, 8].

Post mortem computed tomography (PMCT) enables non-destructive assessment of internal structures and provides quantitative attenuation values that can be used to distinguish gas, fat-like, fluid-like and denser components [9–13]. Recent forensic imaging research has increasingly focused on objective quantification of *post mortem* changes, including radiomics-based approaches to time-since-death estimation [14]. However, the volumetric composition of femoral medullary content during advanced decomposition remains poorly characterised. Attenuation-based segmentation provides a practical way to quantify this content, but the resulting measurements may depend on image reconstruction parameters. Reconstruction kernels influence image noise and spatial resolution [15].

The primary aim of this study was therefore to assess agreement between femoral medullary volumetric fractions obtained from two routinely generated PMCT reconstruction protocols: a soft-tissue reconstruction (ST) and a bone reconstruction (BN). The secondary aim was to explore associations between these fractions and two reference variables: the Radiological Alteration Index (RAI), which quantifies the extent of *post mortem* gas formation on PMCT [16], and an estimated *post mortem* interval (PMI) derived from the date of last contact. We hypothesised that the principal medullary fractions would show high agreement between reconstruction protocols and that some fractions would vary systematically with the degree of cadaveric alteration.

Materials and methods

Study design and population

This retrospective study used PMCT examinations acquired at the *Institut Médico-Légal de* Toulouse, France, between February 2024 and May 2026. Cases were eligible if the medicolegal record described advanced decomposition (putrefaction, mummification or skeletonisation). Exclusion criteria at the individual level were known bone or bone marrow pathology, drowning or prolonged submersion, carbonisation and markedly atypical discovery conditions likely to alter decomposition. Individual femora were excluded from segmentation when they contained prosthetic or osteosynthesis material liable to generate artefacts, metallic foreign bodies affecting the femur, or femoral fractures.

PMCT acquisition

All examinations were performed using a Siemens Somatom Definition AS20 multidetector CT scanner (Siemens Healthineers, Erlangen, Germany). Imaging was acquired in three anatomical blocks with a tube voltage of 140 kV and automatic tube-current modulation. Two reconstructions derived from the same acquisition were evaluated: an ST reconstruction using the Br36s convolution kernel (slice thickness 1.5 mm; increment 1.0 mm) and a BN reconstruction using the Br60s convolution kernel (slice thickness 0.75 mm; increment 0.5 mm). Because kernel, slice thickness and reconstruction increment differed simultaneously, ST and BN were considered complete reconstruction protocols rather than isolated kernel conditions.

Femoral extraction and medullary segmentation

Femoral extraction and medullary segmentation
Femoral diaphysis extraction and medullary cavity segmentation were performed with SegMed (version 3.1.0), a semi-automated module developed for 3D Slicer (version 5.10.0). From an expert-defined cortical seed point, SegMed isolates the diaphyseal cortex using attenuation thresholding (700–2500 HU), estimates the long axis by principal component analysis, and delimits the diaphyseal region using bone-specific anatomical ratios. Medullary content was classified into attenuation-based categories

using the default Hounsfield unit (HU) thresholds implemented in SegMed. These thresholds were applied uniformly to all examinations, without case-specific adjustment. The predefined ranges were: pure gas, − 1000 to − 700 HU; mixed/aerated gas, >−700 to − 350 HU; fat-like marrow, − 200 to − 30 HU; fluid-like content, − 5 to + 20 HU; intermediate-density material, + 21 to + 300 HU; and hyperdense debris, + 301 to + 1200 HU. Residual medullary content comprised cavity voxels remaining after priority extraction of the other classes. Total gas was calculated as the sum of pure and mixed gas. These categories represent CT attenuation classes and should not be interpreted as direct histological tissue labels. Each femur was processed independently on the ST and BN reconstructions, with the diaphyseal region defined separately for each reconstruction protocol. No manual corrections were performed after segmentation. All segmentations were performed by a single operator (S. Chaigneau). A representative example of diaphyseal extraction and attenuation-based medullary segmentation on ST and BN reconstructions is shown in Fig. 1.

Reference variables and final sample

For each class, the volumetric fraction was calculated as the class volume divided by total medullary cavity volume. Eight fractions were analysed: total gas, pure gas, mixed gas, fat-like marrow, fluid, intermediate-density material, residual medullary content and debris. The RAI was assessed according to the method of Egger et al. [16], based on the semiquantitative grading of gas at seven anatomical sites on PMCT: the cardiac cavities, liver parenchyma and vessels, left innominate vein, abdominal aorta, renal parenchyma, third lumbar vertebra (L3), and subcutaneous pectoral tissues. Gas was graded at each site on an ordinal scale from 0 to III, with predefined scores summed to obtain an index ranging from 0 to 100. All RAI assessments were performed by a single operator (S. Chaigneau). To focus on advanced putrefaction, cases with an available RAI < 70 were excluded. In three cases, the RAI could not be calculated because the thoraco-abdomino-pelvic DICOM series was unavailable; these cases were nevertheless retained because advanced putrefaction was clearly documented in the medicolegal record. The estimated *post mortem* interval (PMI) was defined as the number of days between the latest documented last contact and body discovery. The last-contact date was extracted from medicolegal records and police reports and could reflect a witnessed encounter, telephone contact, or indirect evidence such as the collection of postal mail; sources were not weighted by reliability. The resulting interval was therefore treated as an approximate exploratory measure, not a confirmed time since death. Before the final study sample was established, cases with an available estimated PMI greater than 60 days were excluded because observations beyond 60 days were sparse; isolated estimated intervals had reached 187 days before restriction. Individuals without an estimated PMI could still be retained when they met the other eligibility criteria. The final sample comprised 100 individuals (74 males, 26 females; median age 62.5 years, Q1–Q3 51.5–71.8) and 199 femora.

Statistical analysis

Analyses were performed in R (version 4.6.0). Because the RAI, estimated PMI and nearly all volumetric fractions deviated from normality, non-parametric methods were used. ST–BN agreement was assessed

on paired femora using Wilcoxon signed-rank tests. For these paired comparisons, Benjamini–Hochberg false-discovery-rate correction was applied jointly to the 16 tests corresponding to eight volumetric fractions and two femoral sides. Agreement was further quantified using two-way random-effects, absolute-agreement, single-measure intraclass correlation coefficients (ICCs) with 95% confidence intervals. Bland–Altman analysis was also performed, with mean bias calculated as BN minus ST and 95% limits of agreement defined as the mean bias ± 1.96 standard deviations of the paired differences. Spearman rank correlations were calculated between each volumetric fraction and the RAI and estimated PMI, separately for the four combinations of femoral side and reconstruction protocol. Benjamini–Hochberg correction was applied separately to the RAI and estimated PMI correlation families, each comprising 32 comparisons (eight fractions × four series). As a complementary individual-level analysis, available left and right values were averaged within each individual for each reconstruction protocol. When only one femur was available, the corresponding unilateral value was retained. Individuals without any segmented femur for a given reconstruction protocol were excluded from the corresponding analysis. Spearman correlations were then repeated, with Benjamini–Hochberg correction applied separately to the RAI and estimated PMI families, each comprising 16 comparisons (eight fractions × two reconstruction protocols). Statistical significance was defined as an adjusted p value < 0.05.

Results

Study population and medullary composition

The final sample comprised 100 individuals and 199 femora, as one individual had only one lower limb. The 199 available femora corresponded to 398 expected femur-reconstruction combinations (ST and BN). Of these, 390 were successfully segmented (right ST, n = 96; right BN, n = 97; left ST, n = 98; left BN, n = 99). The eight remaining reconstruction series were not segmented because of osteosynthesis material in the right femur, ST field-of-view truncation excluding the femoral diaphysis, corrupted or incomplete image data preventing reliable segmentation, or faulty scan exports. The RAI was available for 97 individuals and the estimated PMI for 64. Across the four series, intermediate-density material was the largest medullary compartment (median fraction approximately 0.31–0.33), followed by residual medullary content (0.19–0.20) and fat-like marrow (0.16–0.18). Total gas represented a median fraction of approximately 0.13–0.16, fluid approximately 0.05, and debris less than 0.01. Gas fractions were strongly right-skewed.

Table 1
Study sample and analysis availability

Characteristic	Value
Individuals	100
Sex	74 males; 26 females
Age	Median 62.5 years (Q1–Q3 51.5–71.8; available for 98/100 individuals)
Femora available	199
RAI available	97 individuals
Estimated PMI available	64 individuals
Right ST series	96
Right BN series	97
Left ST series	98
Left BN series	99

Agreement between reconstruction protocols

Because paired analyses required successful segmentation of both reconstruction protocols for the same femur, the ST–BN comparison included 95 right and 98 left femora. ICCs exceeded 0.94 for total, pure and mixed gas, fat-like marrow, fluid and intermediate-density material on both sides, indicating excellent absolute agreement. The principal exception was residual medullary content on the right (ICC = 0.520, 95% CI 0.356–0.653), while debris showed lower and less stable agreement because of the very small measured volumes. Although Wilcoxon tests identified statistically significant ST–BN differences for most fractions, absolute median differences were ≤ 0.02. The largest systematic offset concerned intermediate-density material, which was approximately 0.02 lower with BN than with ST. Fat-like marrow showed no evidence of a difference between reconstruction protocols on either side. Bland–Altman plots showed generally small biases for most fractions, whereas residual medullary content and debris displayed wider and less stable limits of agreement (Figs. 2 and 3).

Table 2

Paired comparison of medullary volumetric fractions between ST and BN reconstruction protocols. Median diff. = median paired difference (BN–ST); p (BH) = Benjamini–Hochberg-adjusted p value.

Fraction	N	Median ST	Median BN	Median diff.	p (BH)	ICC	95% CI
Right femur							
Total gas	95	0.1351	0.1617	0.0069	< 0.001	0.959	0.936–0.973
Pure gas	95	0.0318	0.0506	0.0065	< 0.001	0.948	0.910–0.969
Mixed gas	95	0.1033	0.1045	−0.0007	0.0143	0.975	0.963–0.983
Fat-like marrow	95	0.1724	0.1721	−0.0027	0.5139	0.979	0.969–0.986
Fluid	95	0.0534	0.0536	0.0013	< 0.001	0.982	0.965–0.990
Intermediate-density	95	0.3288	0.3047	−0.0196	< 0.001	0.983	0.892–0.994
Residual medullary	95	0.1934	0.1974	0.0045	< 0.001	0.520	0.356–0.653
Debris	95	0.0049	0.0026	−0.0020	< 0.001	0.819	0.255–0.932
Left femur							
Total gas	98	0.1253	0.1325	0.0074	< 0.001	0.997	0.990–0.999
Pure gas	98	0.0264	0.0298	0.0065	< 0.001	0.992	0.956–0.997
Mixed gas	98	0.0879	0.0811	−0.0006	0.0450	0.996	0.995–0.998
Fat-like marrow	98	0.1658	0.1633	−0.0015	0.7098	0.976	0.965–0.984
Fluid	98	0.0461	0.0490	0.0028	< 0.001	0.977	0.952–0.988
Intermediate-density	98	0.3332	0.3137	−0.0194	< 0.001	0.979	0.909–0.992
Residual medullary	98	0.1878	0.1938	0.0035	< 0.001	0.944	0.887–0.968
Debris	98	0.0051	0.0029	−0.0019	< 0.001	0.763	0.078–0.914

Associations with RAI and estimated PMI

Gas fractions were positively associated with RAI in all four series (ρ approximately 0.25 – 0.35), with all associations remaining statistically significant after Benjamini-Hochberg correction. Fluid and intermediate-density fractions were negatively associated with RAI, with coefficients of similar magnitude (approximately − 0.27 to − 0.37). The strongest observed associations were total gas in left BN (ρ = 0.351), pure gas in left BN (ρ = 0.347) and intermediate-density material in left ST (ρ = −0.369). In the side-specific analyses, fat-like marrow and debris were not significantly associated with RAI after correction. No correlation between a volumetric fraction and estimated PMI reached significance after correction; the smallest adjusted p value was 0.12. The direction of associations with PMI nevertheless paralleled the RAI pattern, with positive coefficients for gas and negative coefficients for fluid and intermediate-density material (Fig. 4).

The complementary individual-level analysis produced the same overall pattern. For RAI, gas fractions remained positively correlated and fluid and intermediate-density fractions negatively correlated, with significant associations after correction for both reconstruction protocols. A weak negative correlation for debris reached statistical significance only in the individual-level ST analysis (ρ = −0.219, adjusted p = 0.046), but this finding was not reproduced in BN or in the side-specific analyses. No fraction in the individual-level analysis was significantly correlated with estimated PMI (Fig. 5).

Discussion

This study shows that the main attenuation-based components of femoral medullary content can be quantified consistently across two routine PMCT reconstruction protocols in advanced decomposition. Three findings are particularly relevant: agreement was excellent for most medullary fractions; gas fractions were positively associated with RAI while fluid and intermediate-density fractions were negatively associated with RAI; and no fraction showed a statistically robust association with the estimated PMI.

The high ICCs for gas, fat-like marrow, fluid and intermediate-density material indicate that the segmentation is robust to the practical choice between the ST and BN protocols used at our institution. Reconstruction parameters are known to affect quantitative CT measurements [15, 17, 18], and statistically significant paired differences were therefore not unexpected. Their magnitude was nevertheless small. The intermediate-density fraction was approximately 0.02 lower with BN, a difference compatible with the higher spatial resolution and different noise characteristics of sharper reconstructions. Importantly, the two protocols differed not only in convolution kernel but also in section thickness and increment; the study therefore demonstrates agreement between complete routine reconstruction protocols rather than isolating a pure kernel effect.

Residual medullary content and debris were less stable. Residual content is defined by exclusion after classification of the other attenuation classes, while debris represents a very small hyperdense

compartment. Both are therefore sensitive to minor voxel reclassification. These categories should remain exploratory until repeatability and biological validity are evaluated further.

The isolated association between debris and RAI observed in the individual-level ST analysis should be interpreted cautiously. Measurements from the right and left femora are not biologically identical, and side-specific variability in this very small compartment may influence the individual-level summary. The absence of a corresponding association in BN and in the side-specific analyses does not support a robust relationship between debris and radiological alteration.

The association with RAI followed a biologically coherent pattern. Putrefaction produces gas within tissues and vessels [12, 19, 20], and an increase in intramedullary gas with increasing radiological alteration is therefore expected. Fluid and intermediate-density fractions showed inverse associations with RAI, but their biological interpretation is limited by the compositional nature of the measurements. There was no evidence of an association between fat-like marrow and RAI or of a systematic difference between reconstruction protocols. However, the absence of these associations does not establish the biological stability or persistence of adipose marrow during decomposition.

Because medullary fractions share a common denominator, they are compositionally constrained [21]. An increase in the gas fraction may therefore be accompanied by a decrease in other fractions even without a corresponding reduction in their absolute volumes. Accordingly, the inverse associations observed between gas and non-gaseous fractions should not be interpreted as direct evidence of tissue replacement or loss.

The correlations with RAI were statistically significant but moderate ($|\rho|$ approximately 0.25–0.37). This is plausible because decomposition is strongly modulated by temperature, humidity, body characteristics and discovery conditions [1, 4]. A single medullary fraction should therefore not be interpreted as a stand-alone measure of decomposition. Because the RAI and medullary gas fractions quantify related manifestations of putrefactive gas formation, their association is consistent with radiological cadaveric alteration but does not constitute independent validation of medullary composition as a general decomposition marker. Furthermore, these associations do not, by themselves, provide an estimate of elapsed post mortem time.

No fraction was significantly associated with estimated PMI after multiple-comparison correction. This result should be interpreted in light of the available time variable. Estimated PMI was available for only 64 individuals and was derived from the last documented contact rather than from a known time of death. It therefore represents an uncertain proxy for elapsed time, with heterogeneous reliability across cases. This uncertainty may be accentuated in delayed-discovery and solitary-death contexts [22]. In addition, decomposition rate is not a simple function of elapsed time. These sources of measurement error are expected to attenuate time-based associations, while the restriction to PMI ≤ 60 days further narrowed the observable range. Prospective or well-documented retrospective cohorts with accurately known death times are needed before the value of medullary composition for PMI estimation can be assessed.

Several methodological limitations should be acknowledged. All segmentations were performed and all RAI scores were assigned by a single operator; inter-operator reproducibility and intra-operator repeatability remain to be established. Because the diaphyseal regions were defined independently on ST and BN images, minor differences in region delineation may also have contributed to the observed ST–BN differences. The attenuation classes have not been validated against histology or biochemistry and must be interpreted as density-based compartments rather than tissue diagnoses. Age and sex may influence baseline marrow composition [23–25], and the present cohort was predominantly male and relatively old. The selection of cases with advanced radiological alteration restricted the range of decomposition states represented in the cohort and may limit the generalisability of the observed associations to earlier stages of decomposition. Finally, this was a single-centre study using one scanner and two institution-specific reconstruction protocols, so external validation is required.

Future work should combine reproducibility testing, histological or biochemical validation of attenuation classes, multicentre PMCT data and more accurate temporal information. If these requirements are met, quantitative femoral medullary analysis may become a useful complement to established *post mortem* imaging markers, particularly in advanced decomposition and partially skeletonised cases where soft-tissue information is limited.

Conclusion

Semi-automated PMCT segmentation yielded high agreement between the two routine reconstruction protocols for most femoral medullary attenuation fractions. Intramedullary gas, fluid and intermediate-density fractions were associated with radiological cadaveric alteration, suggesting their potential as candidate quantitative imaging markers. However, these associations do not establish a relationship with elapsed post mortem time, and no fraction was significantly associated with estimated PMI after multiple-comparison correction. Further studies should assess intra- and inter-operator reproducibility, validate attenuation-based classes against biological reference methods, and evaluate temporal associations in cohorts with accurately known PMIs before application to time-since-death estimation.

Declarations

Competing interests:

The authors declare no competing financial or non-financial interests directly related to this work.

Ethics approval:

No ethics committee approval was sought. All PMCT examinations had been performed for medicolegal purposes, independently of the present research, as part of judicial death investigations under the authority of the competent judicial authorities. The present study involved only the secondary use of fully anonymised data and no additional procedure was performed on the deceased. The study did not

constitute research involving the human person (*recherche impliquant la personne humaine*, RIPH) under French law and was conducted in accordance with the French CNIL MR-004 reference methodology applicable to research not involving the human person and with Article 86 of the French Data Protection Act concerning the use of data relating to deceased individuals.

Clinical trial number

Not applicable.

Consent to participate:

Not applicable. This retrospective study involved the secondary use of previously acquired *post mortem* data and did not involve living participants. No additional procedure was performed for research purposes. According to the applicable French regulatory framework, specific informed consent was not required for this study.

Consent to publish:

Not applicable. The manuscript contains no identifying information or identifiable images of individual deceased persons.

Funding:

No funds, grants, or other support were received for conducting this study.

Author Contribution

S.C.: Investigation, data curation, formal analysis, visualization, writing – original draft. F.S.: Conceptualization, supervision, writing – review and editing. P.N.: Conceptualization, methodology, software (SegMed), supervision, writing, – review and editing. F.D.: Conceptualization, supervision, writing – review and editing. N.T.: Conceptualization, supervision, writing – review and editing.

Data availability:

The anonymised data analysed in this study are not publicly available because they originate from confidential medicolegal records and *post mortem* imaging data and remain subject to institutional, legal and data-protection restrictions.

Code availability:

The SegMed module used for semi-automated segmentation in this study is not publicly available at present.

References

1. Franceschetti L, Amadasi A, Bugelli V et al (2023) Estimation of late postmortem interval: where do we stand? A literature review. Biology 12:783. https://doi.org/10.3390/biology12060783
2. Singh J, Kumar A, Trivedi S, Pandey SK (2025) Advancements in estimating post-mortem interval in medico-legal practice: a comprehensive review. Leg Med 75:102627. https://doi.org/10.1016/j.legalmed.2025.102627
3. Lee Goff M (2009) Early post-mortem changes and stages of decomposition in exposed cadavers. Exp Appl Acarol 49:21–36. https://doi.org/10.1007/s10493-009-9284-9
4. Quatrehomme G (2015) Traité d'anthropologie médico-légale. De Boeck Supérieur, Louvain-la-Neuve. ISBN 978-2-8041-8469-8
5. Wescott DJ (2019) Postmortem change in bone biomechanical properties: loss of plasticity. Forensic Sci Int 300:164–169. https://doi.org/10.1016/j.forsciint.2019.04.017
6. Schmidt V-M, Zelger P, Woess C et al (2022) Application of micro-computed tomography for the estimation of the post-mortem interval of human skeletal remains. Biology 11:1105. https://doi.org/10.3390/biology11081105
7. Tattoli L, Tsokos M, Sautter J et al (2014) Postmortem bone marrow analysis in forensic science: Study of 73 cases and review of the literature. Forensic Sci Int 234:72–78. https://doi.org/10.1016/j.forsciint.2013.10.040
8. Sakr MF, El-Khalek AMA, Mohammad NS et al (2024) Estimation of postmortem interval using histological and oxidative biomarkers in human bone marrow. Forensic Sci Med Pathol 20:910–919. https://doi.org/10.1007/s12024-023-00753-9
9. Dedouit F, Ducloyer M, Elifritz J et al (2025) The current state of forensic imaging – recommended radiological tools and international guidelines. Int J Legal Med 139:2219–2231. https://doi.org/10.1007/s00414-025-03465-7
10. Norberti N, Tonelli P, Giaconi C et al (2019) State of the art in post-mortem computed tomography: a review of current literature. Virchows Arch 475:139–150. https://doi.org/10.1007/s00428-019-02562-4
11. Grabherr S, Egger C, Vilarino R et al (2017) Modern post-mortem imaging: an update on recent developments. Forensic Sci Res 2:52–64. https://doi.org/10.1080/20961790.2017.1330738
12. Cartocci G, Santurro A, Neri M et al (2019) Post-mortem computed tomography (PMCT) radiological findings and assessment in advanced decomposed bodies. Radiol med 124:1018–1027. https://doi.org/10.1007/s11547-019-01052-6
13. Zech W-D, Jackowski C, Buetikofer Y, Kara L (2014) Characterization and differentiation of body fluids, putrefaction fluid, and blood using Hounsfield unit in postmortem CT. Int J Legal Med

128:795–802. https://doi.org/10.1007/s00414-014-1030-0

14. Klontzas ME, Leventis D, Spanakis K et al (2023) Post-mortem CT radiomics for the prediction of time since death. Eur Radiol 33:8387–8395. https://doi.org/10.1007/s00330-023-09746-2
15. Sandbukt Johnsen A-M, Fenn JM, Henning MK, Hauge IH (2023) Optimization of chest CT protocols based on pixel image matrix, kernels and iterative reconstruction levels – A phantom study. Radiography 29:752–759. https://doi.org/10.1016/j.radi.2023.05.005
16. Egger C, Vaucher P, Doenz F et al (2012) Development and validation of a postmortem radiological alteration index: the RA-Index. Int J Legal Med 126:559–566. https://doi.org/10.1007/s00414-012-0686-6
17. Matheson BE, Boyd SK (2025) Establishing the effect of computed tomography reconstruction kernels on the measure of bone mineral density in opportunistic osteoporosis screening. Sci Rep 15:5449. https://doi.org/10.1038/s41598-025-88551-x
18. Krishnan AR, Xu K, Li TZ et al (2024) Lung CT harmonization of paired reconstruction kernel images using generative adversarial networks. Med Phys 51:5510–5523. https://doi.org/10.1002/mp.17028
19. Byard RW (2025) Artefacts due to putrefactive gas production – an overview. Med Sci Law 65:65–70. https://doi.org/10.1177/00258024241275894
20. Gelius T, Möllby R, Bergdahl J et al (2026) Medico-legal interpretations of gas on postmortem CT: a scoping review. Int J Legal Med. https://doi.org/10.1007/s00414-026-03930-x
21. Aitchison J (1982) The Statistical Analysis of Compositional Data. J Royal Stat Soc Ser B: Stat Methodol 44:139–160. https://doi.org/10.1111/j.2517-6161.1982.tb01195.x
22. Byard RW (2025) The forensic implications of lonely deaths (*Kodokushi*) – A South Australian study. J Forensic Leg Med 109:102799. https://doi.org/10.1016/j.jflm.2024.102799
23. Baum T, Rohrmeier A, Syväri J et al (2018) Anatomical variation of age-related changes in vertebral bone marrow composition using chemical shift encoding-based water–fat magnetic resonance imaging. Front Endocrinol 9:141. https://doi.org/10.3389/fendo.2018.00141
24. Griffith JF, Yeung DKW, Ma HT et al (2012) Bone marrow fat content in the elderly: A reversal of sex difference seen in younger subjects. J Magn Reson Imaging 36:225–230. https://doi.org/10.1002/jmri.23619
25. Małkiewicz A, Dziedzic M (2012) Bone marrow reconversion - imaging of physiological changes in bone marrow. Pol J Radiol 77:45–50. https://doi.org/10.12659/pjr.883628

Figures

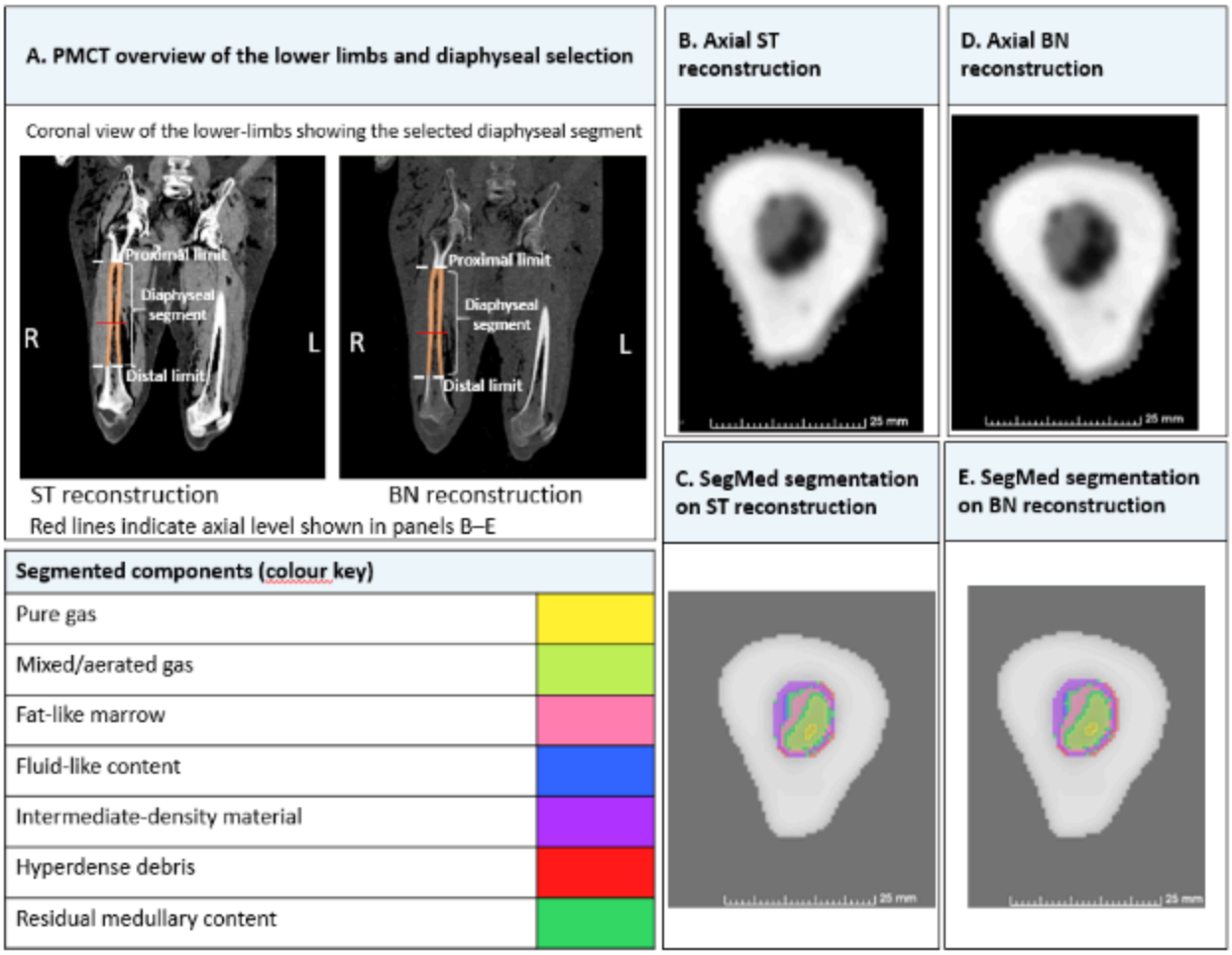


Figure 1

Representative PMCT images and SegMed segmentation of the femoral diaphysis in advanced decomposition. (A) Coronal PMCT overview showing the selected diaphyseal segment on ST and BN reconstructions. Red lines indicate the axial level displayed in panels B–E. (B) Axial ST reconstruction. (C) Corresponding SegMed segmentation on the ST reconstruction. (D) Axial BN reconstruction. (E) Corresponding SegMed segmentation on the BN reconstruction. Colours indicate the attenuation-based medullary components used for volumetric analysis. Cortical bone is displayed in white and was not included among the analysed medullary fractions.

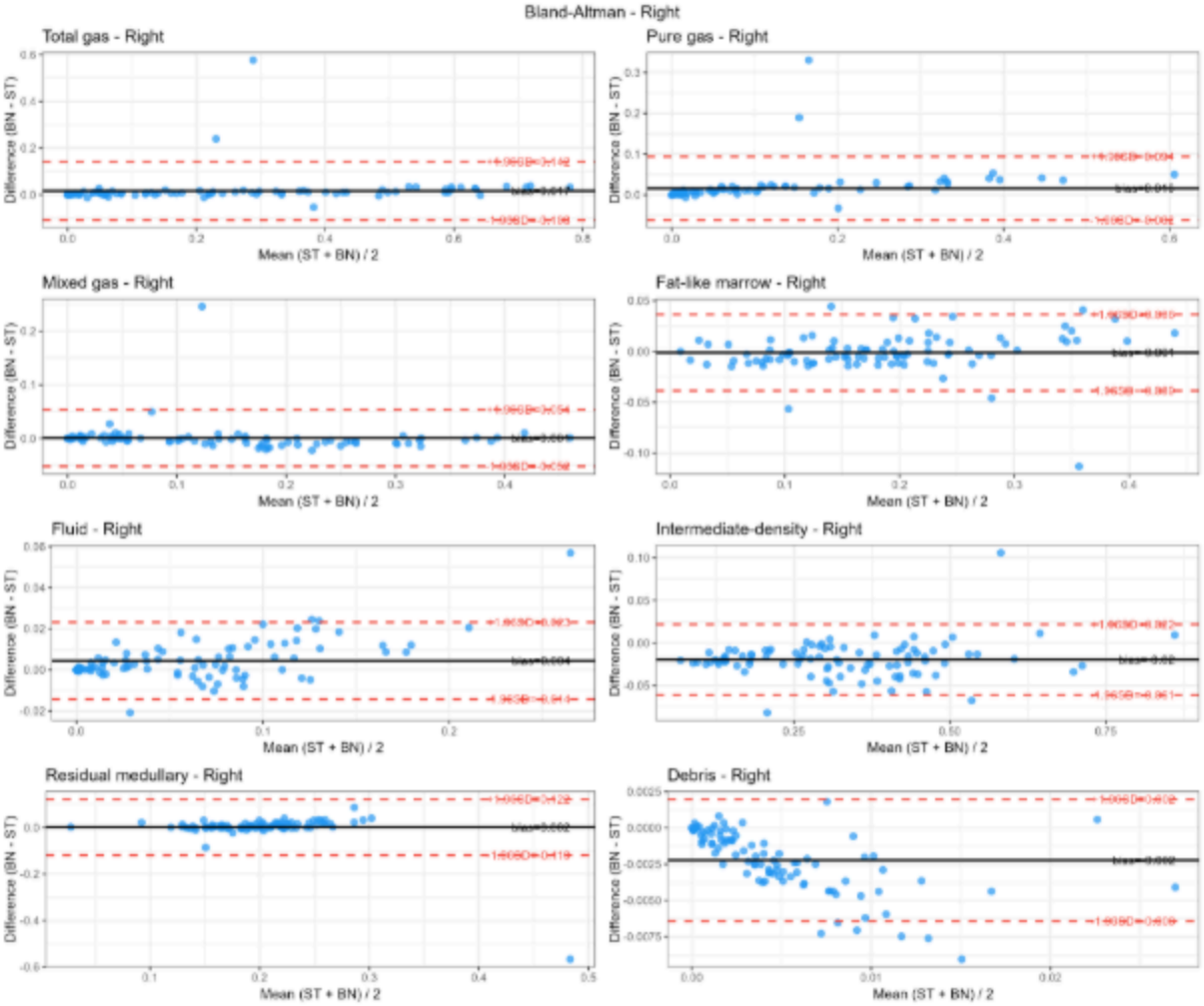


Figure 2

Bland–Altman plots comparing ST and BN reconstruction protocols for the eight volumetric fractions of the right femur. The x-axis shows the mean of the two reconstruction measurements and the y-axis the difference (BN–ST). Solid lines indicate mean bias and dashed lines the 95% limits of agreement

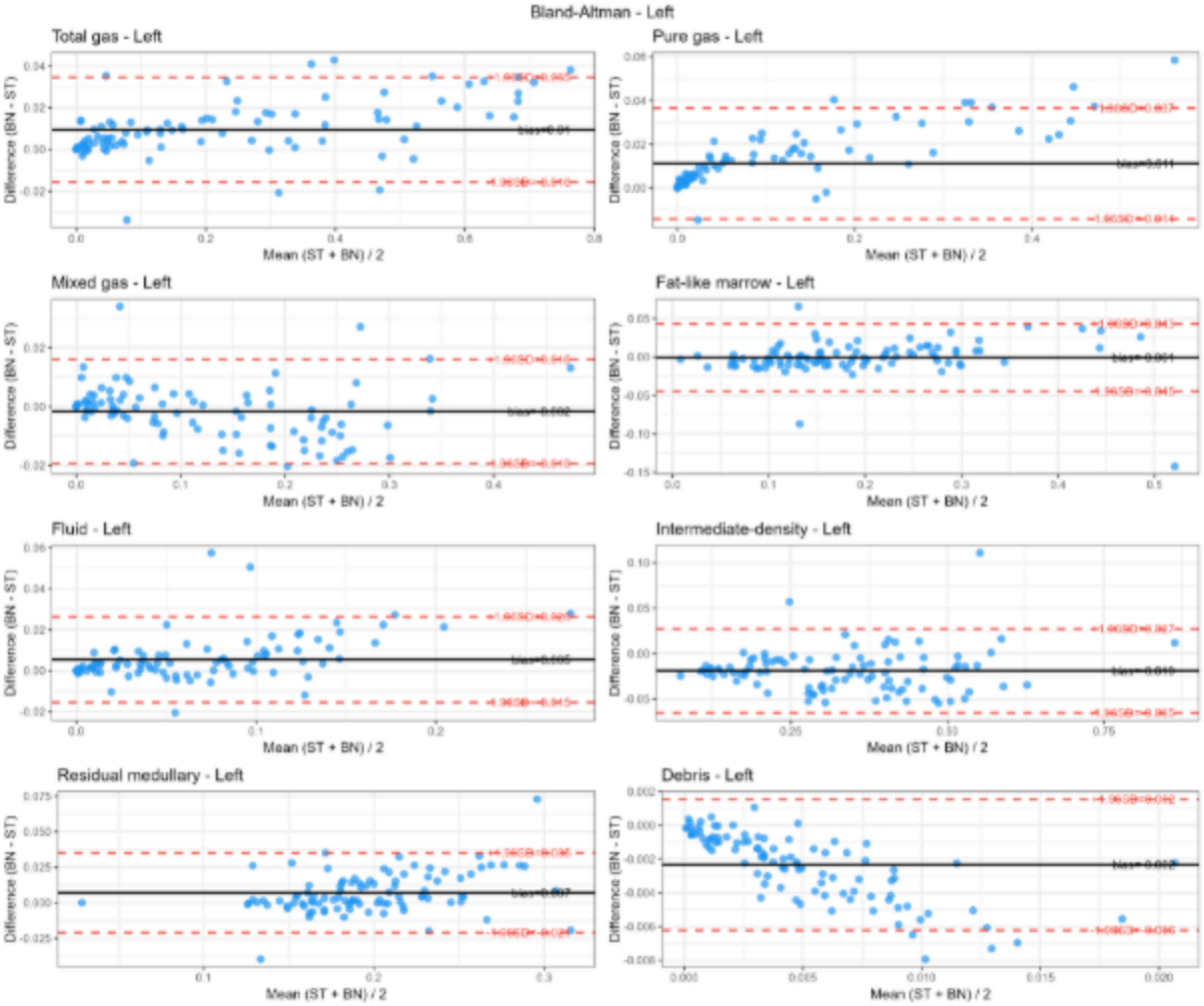


Figure 3

Bland–Altman plots comparing ST and BN reconstruction protocols for the eight volumetric fractions of the left femur. The x-axis shows the mean of both reconstructions and the y-axis the difference (BN–ST). Solid lines indicate mean bias and dashed lines the 95% limits of agreement

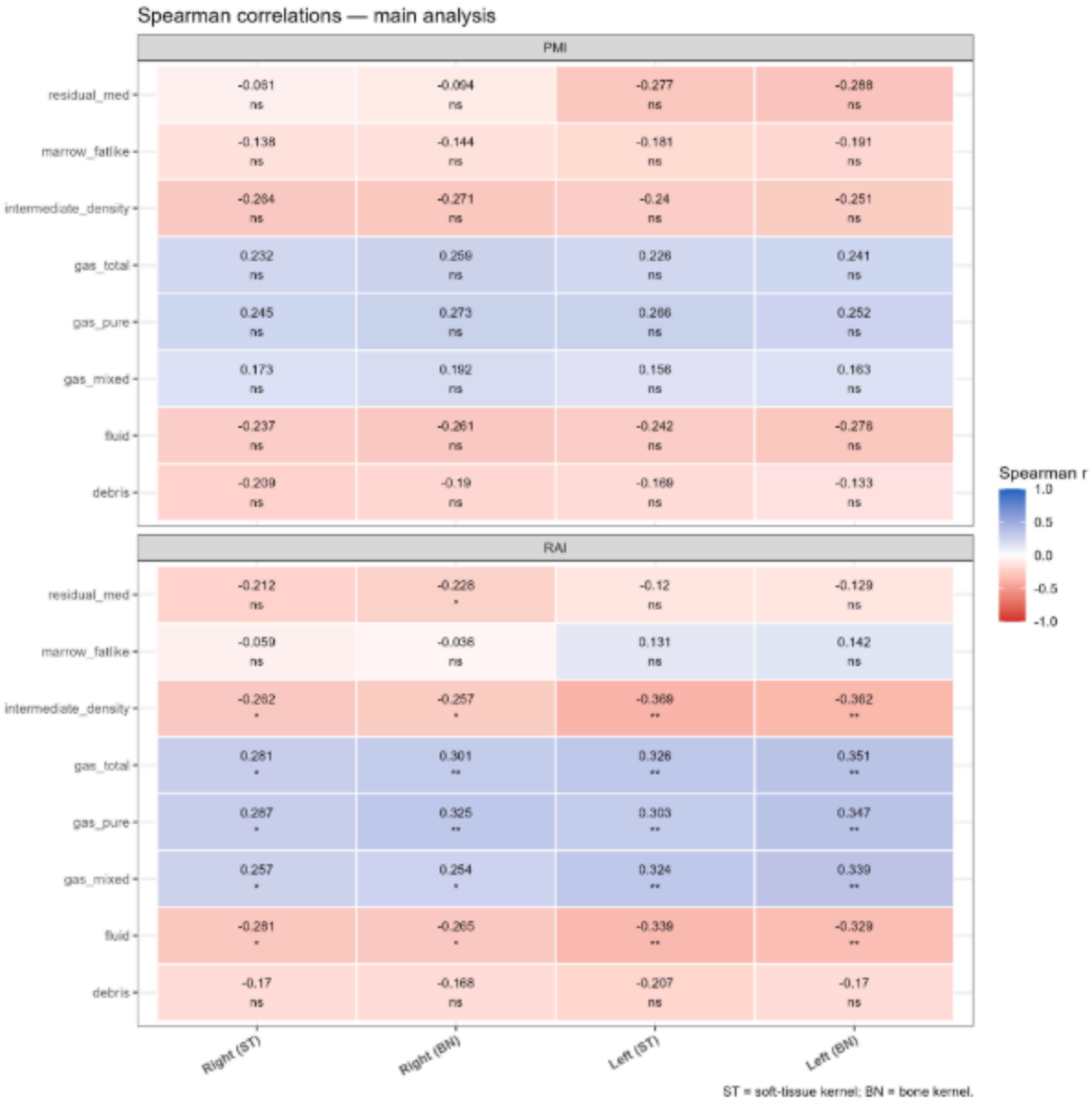


Figure 4

Heatmap of Spearman rank correlations between medullary volumetric fractions and estimated PMI (upper panel) and RAI (lower panel), by femoral side and reconstruction protocol. Asterisks indicate significance after Benjamini–Hochberg correction (* adjusted p < 0.05, ** adjusted p < 0.01, *** adjusted p < 0.001).

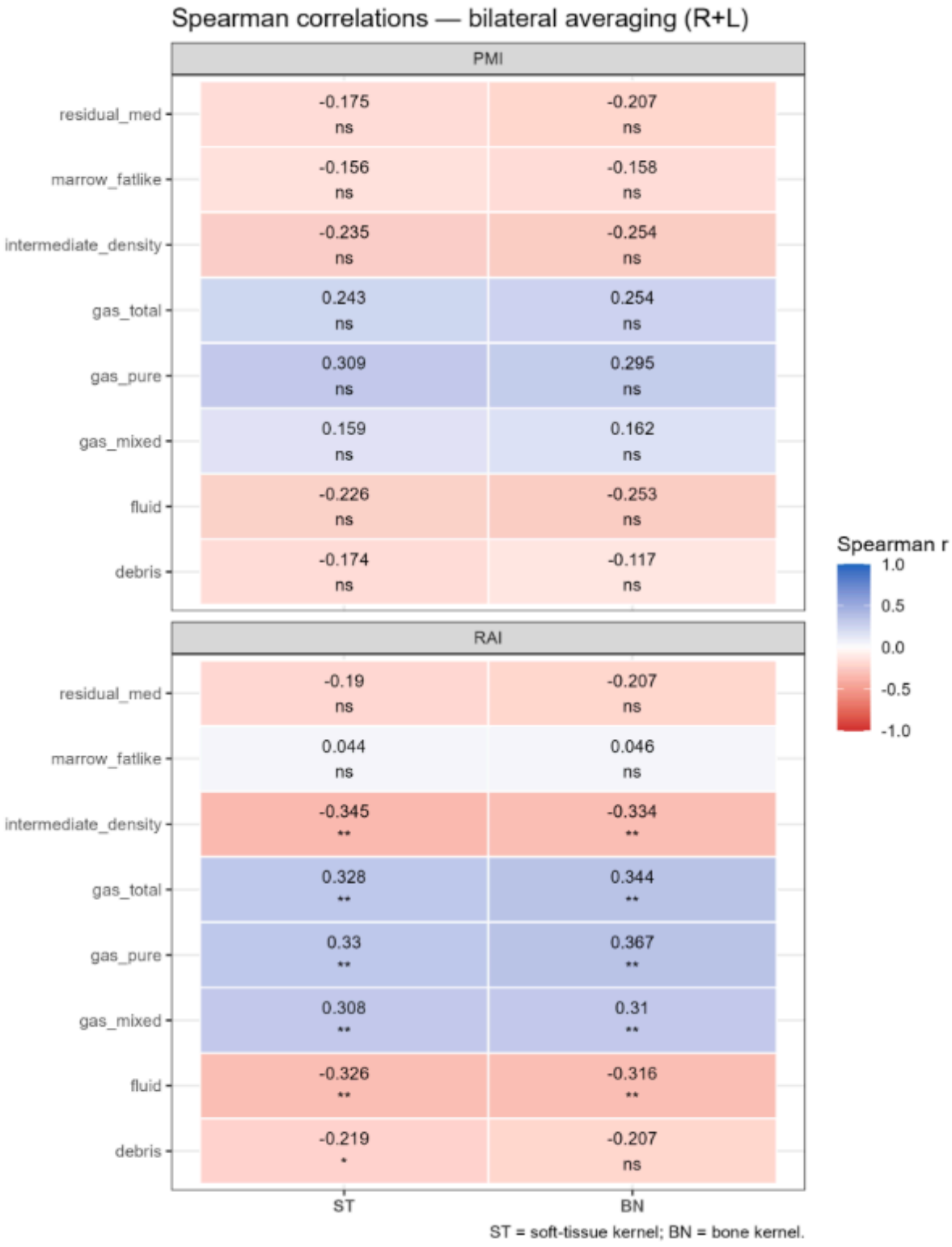


Figure 5

Heatmap of Spearman rank correlations based on individual-level volumetric fractions, obtained by averaging left and right measurements when both were available and retaining the unilateral value otherwise, shown separately for ST and BN reconstruction protocols. Asterisks indicate significance after Benjamini–Hochberg correction (* adjusted p < 0.05, ** adjusted p < 0.01, *** adjusted p < 0.001).